Ozonolysis of Mixed Oleic-Acid/Stearic-Acid Particles: Reaction Kinetics and Chemical Morphology

Y. Katrib,[†] G. Biskos,[†] P. R. Buseck,[‡] P. Davidovits,[§] J. T. Jayne,[||] M. Mochida,[†,⊥] M. E. Wise,[‡] D. R. Worsnop,[||] and S. T. Martin*[,†]

Division of Engineering and Applied Sciences, Harvard University, Cambridge, Massachusetts 02138; Department of Geological Sciences and Department of Chemistry and Biochemistry, Arizona State University, Tempe, Arizona 85287; Chemistry Department, Boston College, Chestnut Hill, Massachusetts 02467; Aerodyne Research, Inc., Billerica, Massachusetts 08121; and Institute of Low-Temperature Science, Hokkaido University, Sapporo, 060-0819, Japan

Received: August 21, 2005; In Final Form: October 8, 2005

The ozonolysis of mixed oleic-acid/stearic-acid (OL/SA) aerosol particles from 0/100 to 100/0 wt % composition is studied. The magnitude of the divergence of the particle beam inside an aerosol mass spectrometer shows that, in the concentration range 100/0 to 60/40, the mixed OL/SA particles are liquid prior to reaction. Upon ozonolysis, particles having compositions of 75/25 and 60/40 change shape, indicating that they have solidified during reaction. Transmission electron micrographs show that SA(s) forms needles. For particles having compositions of 75/25, 60/40, and greater SA content, the reaction kinetics exhibit an initial fast decay of OL for low O_3 exposure with no further loss of OL at higher O_3 exposures. For compositions from 50/50 to 10/90, the residual OL concentration remains at 28 ± 2% of its initial value. The initial reactive uptake coefficient for O_3, as determined by OL loss, decreases linearly from 1.25 (±0.2) × 10^{-3} to 0.60 (±0.15) × 10^{-3} for composition changes of 100/0 to 60/40. At 50/50 composition, the uptake coefficient drops abruptly to 0.15 (±0.1) × 10^{-3}, and there are no further changes with increased SA content. These observations can be explained with a combination of three postulates: (1) Unreacted mixed particles remain as supersaturated liquids up to 60/40 composition, and the OL in this form rapidly reacts with O_3. (2) SA, as it solidifies, locks into its crystal structure a significant amount of OL, and this OL is completely inaccessible to O_3. (3) Accompanying crystallization, some stearic acid molecules connect as a filamentous network to form a semipermeable gel containing liquid OL but with a reduced uptake coefficient because of the decrease in molecular diffusivity in the gel. An individual particle of 50/50 to 90/10 is hypothesized as a combination of SA crystals having OL impurities (postulate 2) that are partially enveloped by an SA/OL gel (postulate 3) to explain (a) the abrupt drop in the uptake coefficient from 60/40 to 50/50 and (b) the residual OL content even after high ozone exposure. The results of this study, pointing out the important effects of particle phase, composition, and morphology on chemical reactivity, contribute to an improved understanding of the aging processes of atmospheric aerosol particles.

1. Introduction

Atmospheric particles directly and indirectly affect global climate[1−5] and have a primary role in regional issues of air pollution, visibility, and human health.[6] Atmospheric particles have a variety of shapes, dimensions, and chemical compositions, and these physicochemical properties evolve (i.e., "age") during transport of the particles through the atmosphere, in part because of the chemical reactions of particle-phase organic molecules with gas-phase atmospheric oxidants.[7−10] On a global average, ozone (O_3) is an important reactant for oxidant-induced aging of atmospheric particles.[11] Ozone is a selective agent for the unsaturated bonds of organic molecules and may diffuse a considerable distance into particles prior to reaction.

The reaction of oleic acid ($C_{18}H_{34}O_2$; *cis*-octadec-9-enoic acid) with ozone has recently emerged as a model system for studying the products and mechanisms of atmospheric chemical oxidation of organic particles. Reactive uptake coefficients,[12−20] product mechanisms,[17−19,21−24] particle hygroscopicity,[24,25] particle density,[26] and particle cloud-condensation-nuclei (CCN) activity[27] have been studied. The reaction proceeds via the addition of ozone to the double bond of oleic acid, which yields a primary ozonide (molozonide).[28] This high-energy molecule rapidly decomposes into stable products such as nonanal, 9-oxononanoic acid, nonanoic acid, and azelaic acid as well as stabilized Criegee intermediates (SCI). The SCI react[18,19,21,23,24] with carbonyl functional groups to form secondary ozonides, with carboxylic acid groups to form α-acyloxyalkyl hydroperoxides, and with other SCI to form cyclic diperoxides. Additional SCI can continue reactions with some classes of α-acyloxyalkyl hydroperoxides and secondary ozonides, especially those containing acid and carbonyl functionalities, to produce oligomerization products.[24]

Oleic acid occurs widely in atmospheric particles.[29−32] Oleic acid, present in the triglycerides used in energy storage by eukaryotes (i.e., in the fats and oils of animals and plants) and in the phospholipids of their biological membranes, is the most abundant unsaturated fatty acid in living bodies.[33,34] As a natural

* To whom correspondence should be addressed. E-mail: scot_martin@harvard.edu. Web: www.deas.harvard.edu/environmental-chemistry.
[†] Harvard University.
[‡] Arizona State University.
[§] Boston College.
[||] Aerodyne Research, Inc.
[⊥] Institute of Low-Temperature Science.

10.1021/jp054714d CCC: $30.25
Published on Web 11/10/2005

product, oleic acid occurs in the fats and oils used in cooking. For example, olive oil is 85% oleic acid while lard and butter are 48% and 27%, respectively. The high temperatures used in cooking, which range from a minimum of 65−70 °C for recommended internal temperatures of meat to 150−175 °C for surface temperatures of griddles to 300−350 °C for surface temperatures of charbroilers, volatilize the saturated and unsaturated fatty acids. Upon cooling, these relatively nonvolatile acids condense and contribute to primary organic aerosol. The saturated fatty acids include the series lauric (C_{12}), myristic (C_{14}), palmitic (C_{16}), and stearic (C_{18}) acids; the unsaturated fatty acids include oleic and linoleic acids. For these reasons, the concentration of oleic acid in urban aerosol has been suggested as a quantitative marker of the contribution of meat cooking to particulate matter (PM) air pollution.[30,32]

The use of oleic acid as a quantitative marker is predicated on the assumption that it is inert to atmospheric transformations. Although atmospheric measurements indicate that particle-phase oleic acid has a lifetime of days in urban environments,[30,32] results of the numerous recent laboratory studies employing pure oleic acid particles suggest that, on the contrary, particle-phase oleic acid in a typical urban environment should react with ozone and disappear within several minutes.[12,14] Field and laboratory studies therefore differ significantly on the rates of particle aging.

A key difference between the laboratory and the atmosphere is that most laboratory studies have been performed with pure oleic acid particles whereas oleic acid in atmospheric particles is mixed with 100's to 1000's of other organic molecules.[35−37] The chemical matrix in which an organic molecule finds itself can greatly alter its chemistry: (1) The bimolecular rate constant of ozone with oleic acid may change, especially if the dimer structure[38−40] of pure liquid oleic acid is disrupted. (2) The pathways of the reaction may be altered by the reaction of the SCI with functional groups of the matrix. (3) Oleic acid may be trapped within solid phases and not accessible to ozone. The first two possibilities seem unlikely to alter reaction rates sufficiently to account for the differences in lifetime between the laboratory and field measurements. To address the third possibility using a model system, we present in this paper the results of our study on the ozonolysis of oleic acid mixed with stearic acid. At 298 K, the equilibrium composition of these particles is a liquid phase of 96% (w/w) oleic acid in contact with a pure phase of solid stearic acid.[41] We compare our results to those of other recent laboratory studies focusing on the effects of possible solid phases on the reactions of oleic acid.[19,20,42]

2. Experimental Section

The experimental apparatus is shown in Figure 1. Solutions of oleic-acid/stearic-acid were atomized. In the case of the kinetics experiments utilizing the aerosol mass spectrometer (AMS), 300-nm mobility diameter particles were selected using a differential mobility analyzer (DMA). For particles collected by electrostatic precipitation (EPS) and imaged by transmission electron microscopy (TEM), the in-line DMA was removed and a polydisperse aerosol was collected. For both the kinetics experiments and the particle imaging, the aerosol was exposed to ozone to cause the ozonolysis of oleic acid. Details of these experimental procedures are provided below.

For atomization to form an aerosol, oleic acid (OL) (>99% purity, Aldrich) and stearic acid (SA) (>99% purity, Aldrich) were dissolved in weight percent mixing ratios of 100/0 to 0/100 OL/SA into 100 mL of methanol (HPLC high purity) as 1 wt % total solute. This solution was atomized (TSI 3076) into an aerosol flow (0.4 Lpm ultrapure N_2) leading to the generation

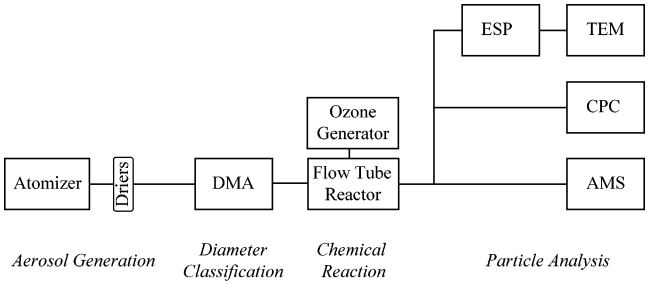

Figure 1. Schematic diagram of experimental system for particle generation, sizing, processing, and analysis. Key: OL, oleic acid; SA, stearic acid; DMA, differential mobility analyzer; AMS, aerosol mass spectrometer; CPC, condensation particle counter; ESP, electrostatic precipitator; TEM, transmission electron microscope.

of a polydisperse distribution of particles. Two 1-m diffusion driers (0.5-in. i.d.) filled with anhydrous calcium sulfate were placed at the exit of the atomizer to absorb methanol evaporated from the aerosol particles. The log−normal size distribution of the dried aerosol had a geometric mean mobility diameter of 100 nm and a geometric standard deviation of 1.5. Hearn and Smith[18] and Broekhuizen et al.[27] have shown that any residual methanol in particles prepared by these methods does not affect the kinetics of the uptake of ozone, although hygroscopic growth is affected.[27]

For the kinetics experiments, nearly monodisperse 300-nm mobility diameter particles were selected by a differential mobility analyzer (DMA; TSI model 3071A).[43] A 10:1 sheath-to-polydisperse aerosol flow was used in the DMA, and a geometric standard deviation of 1.1 was obtained for the size-selected aerosol size distribution. At the exit of the DMA, in a 45-cm long flow tube (0.5-in. i.d.) the particles were exposed to ozone of variable concentration (1 to 50 ppmV; 2.5×10^{13} to 1.25×10^{15} molec cm^{-3}) in 1 atm of 98% N_2 and 2% O_2 for 7 s at a relative humidity under 1% and 298 K.[22,26] The particles were then analyzed using an Aerodyne aerosol mass spectrometer (0.1 Lpm) with an electron impact ionization of 70 eV.[22,44,45] The AMS measured the total aerosol particle mass, recorded the particle mass spectrum, and provided information on the particle shape.

Information on particle shape was obtained by measuring the divergence of the particle beam inside the AMS.[26,44,46] The efficiency with which particles are focused and directed to the vaporizer of the AMS is determined by the aerodynamic lens system[47] and the morphology of the particles.[46] Nonspherical particles are not focused as efficiently as spherical particles because of asymmetric lift forces. To measure the beam divergence, we precisely positioned a beam attenuation device (viz. a 0.3-mm diameter wire) across the path of the particle beam downstream of the lens exit and measured the changes in aerosol mass with changes in wire position. The wire and the vaporizer were 353 mm and 450 mm downstream of the lens exit, respectively.

In a split flow to that entering the AMS (Figure 1), a condensation particle counter (CPC; TSI model 3022A)[48] (0.3 Lpm) measured the aerosol particle number concentration, which varied between 0.5 and 3.0×10^4 particles·cm^{-3} during the course of the experiments. In agreement with this value, the particle mass concentration in the aerosol varied from 70 to 380 μg m^{-3} prior to ozone exposure, as measured by the AMS. For comparison, the equilibrium gas-phase concentration of oleic acid in the aerosol should be 2.4 μg m^{-3} at 298 K given a vapor pressure of 2.1×10^{-10} atm (5.3×10^9 molec cm^{-3}).[49]

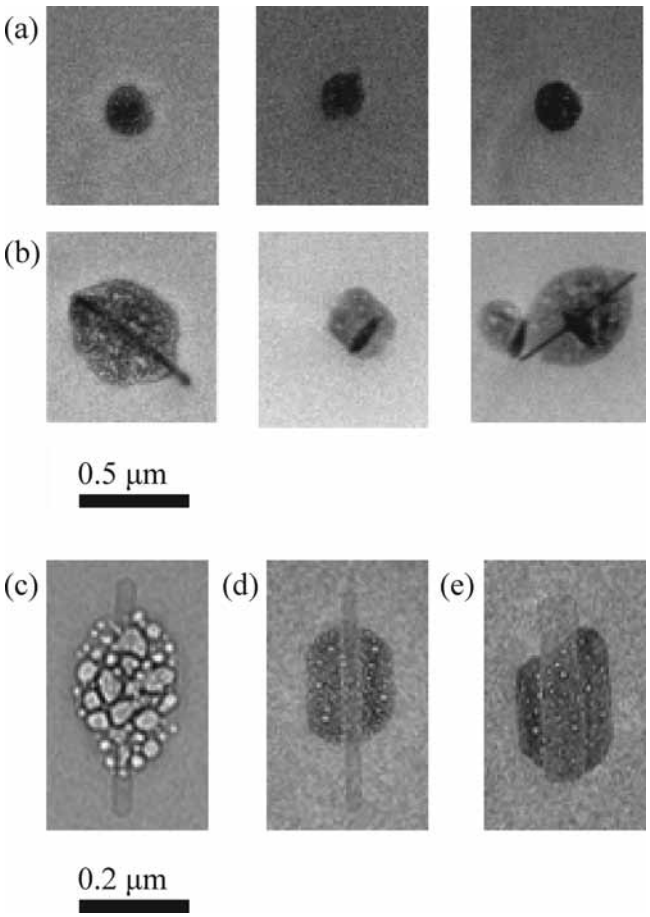

Figure 2. Transmission electron micrographs of collected particles: (a) three examples of 100/0 OL/SA particles collected after reaction with ozone at 298 K and 1% relative humidity; (b) similar examples for 90/10 particles; (c−e) similar examples for 80/20, 50/50, and 30/70 particles, respectively. Needles of stearic acid are apparent in (b)−(e). Key: OL, oleic acid; SA, stearic acid. "90/10" denotes particles of 90 wt % oleic acid and 10 wt % stearic acid. Particle composition is accurate within 1 wt %.

The aerosol collected and imaged by TEM employed the same procedures as described above except that the DMA was removed so that a polydisperse aerosol was analyzed. The polydisperse aerosol was passed through a ^{85}Kr neutralizer (TSI model 3077) to establish a Boltzmann charge distribution on the particles.[50] The positively charged particles of the aerosol were deposited for 6 min on TEM grids (Ted Pella 1820; Formvar layer not removed) by the TSI electrostatic nanoparticle precipitator (TSI model 3089) (1 Lpm flow rate and 10 kV collection voltage). A FEI Tecnai F20 transmission electron microscope, operated at 200 kV and 8300 to 21 000 times magnification and employing a single-tilt sample holder at room temperature, was used to image the deposited particles within 48 to 72 h of collection. Imaging conditions were adjusted to obtain high-quality images of the particles while limiting beam damage. Specifically, the particles were imaged using a dose rate of 3 to 20 electrons Å^{-2} s^{-1} and an exposure time of 1 s. Nevertheless, because organic particles are highly beam sensitive, some damage occurred and could be observed in serial images of the same particle.

3. Results

Transmission electron micrographs are shown in Figure 2 for 100/0, 90/10, 80/20, 50/50, and 30/70 OL/SA particles collected after exposure to ozone. Particles deposited on the TEM grid early in the collection procedure were exposed to 43 ppm (1.1×10^{15} molec cm^{-3}) ozone for up to 6 min; particles deposited late in the collection procedure were exposed for under 30 s. Although the morphology of the stearic acid in the in situ aerosol particles could be different from that after collection and storage on a TEM substrate, the images show that stearic acid forms solid needles with high aspect ratios. The aspect ratio increases as the weight percent stearic acid decreases. The stearic acid needles are partially enveloped in an apparent liquid medium. This liquid medium rapidly decomposes under the electron beam, giving the appearance of bubbles. Further consecutive images (not shown) lead initially to the complete breakdown and evaporation of the liquid layer, which with further imaging is followed by destruction of the stearic acid needles. This phenomenon is explained by damage induced by the electron beam, such as ionization and localized heating. The ratio of the size of the SA needles to the size of the liquid envelope increases steadily for decreasing initial OL/SA ratio, as expected.

A protocol of 36 samples, in which collection times and OL/SA ratios were systematically varied, yielded images only of SA needles and no apparent liquid in the absence of ozone exposure. This result can be explained by simple evaporation of oleic acid. Although this substance is typically considered nonvolatile, in fact its vapor pressure at room temperature corresponds to 2.4 μg m^{-3}, and tandem-DMA experiments in the thesis of Rader show that 100-nm oleic acid particles evaporate by 25% within two min.[49] Therefore, the appearance of liquid regions in Figure 2 is highly significant, indicating a large reduction in the volatility of the ozonolysis products compared to oleic acid. Most notably, Figure 2a shows the apparent liquid residual after ozonolysis of pure oleic acid particles. This decreased volatility is consistent with the report of Hung et al.[24] of increases in viscosity of 1-mm OL particles after ozonolysis. The offered explanation, supported by LC-MS and IR results, was polymerization through ester linkages of α-acyloxyalkyl hydroperoxides.[24] Katrib et al.,[22] Hearn and Smith,[17] Zahardis et al.,[23] and Ziemann[19] also report molecular mass peaks greater than the parent ion peak of oleic acid, findings which suggest that linking reactions occur and result in chemical products of reduced volatility.

A representative particle mass spectrum indicating the loss of oleic acid is shown in Figure 3 for 75/25 OL/SA aerosol particles. The oleic acid molecular peak of 282 amu is still present in the condensed phase even after extensive ozone exposure (Figure 3a versus Figure 3b). The mass spectrum of pure stearic acid does not have a peak at 282 amu. Therefore, although oleic acid does decay, it does not disappear completely for 75/25 OL/SA aerosol particles.

The results for other ozone exposures and other OL/SA particles compositions are shown in Figure 4. Oleic acid reacts completely only for 100/0 and 90/10 particles. As the SA content increases from 90/10 to 50/50, the residual oleic acid content at high ozone exposure continues to increase. For compositions from 50/50 to 10/90, the residual oleic acid concentration is constant within experimental capability at 25 to 30% of its initial value. Moreover, the normalized rate of initial oleic acid loss decreases from 90/10 to 50/50 OL/SA but then remains constant for 50/50 to 10/90 OL/SA. For all compositions having an SA content greater than 90/10, the reaction kinetics appear to have a two-step behavior, showing an initial fast decay for low ozone exposure followed by an apparent absence of further reaction at high ozone exposure.

Ziemann[19] similarly reports that oleic acid in 10/90 aerosol particle mixtures of OL/C_{15}COOH and OL/C_{16}COOH reacts to

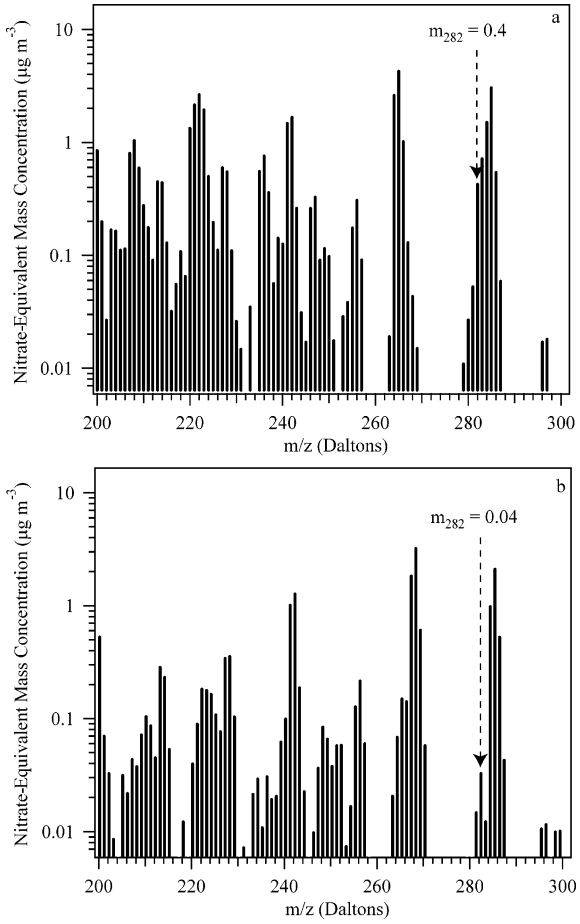

Figure 3. Mass spectra of 75/25 OL/SA aerosol particles: (a) unreacted particles; (b) particles reacted with ozone for 300×10^{-6} atm·s at 298 K and 1% relative humidity (7-s reaction time). Aerosol particles had 300-nm mobility diameter prior to reaction (geometric standard deviation of 1.1). Spectrum b shows that the oleic acid molecular peak of 282 amu is still present in the condensed phase even after extensive ozone exposure. The molecular peak of stearic acid is at 284 amu.

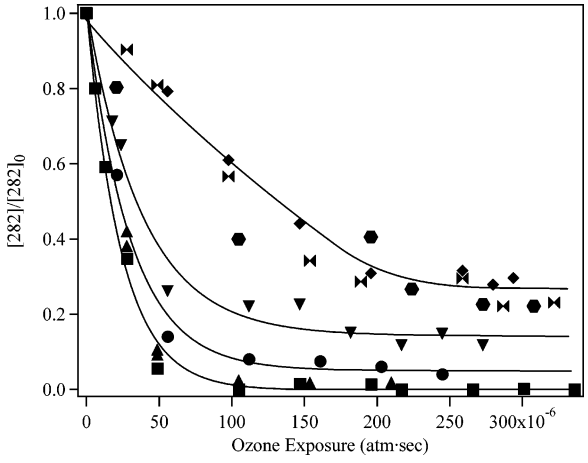

Figure 4. Decay of the molecular peak of oleic acid ($[282]/\{[282]_0$) as a function of ozone exposure. Reaction time is fixed at 7 s, and ozone concentration is varied. Key: pure oleic acid (■); 90/10 OL/SA (▲); 75/25 OL/SA (●); 60/40 OL/SA (▼); 50/50 OL/SA (◆); 30/70 OL/SA (⋈); 10/90 OL/SA (⬣). Lines are to guide the eye and do not represent a model fit. See further details in the caption of Figure 3.

65% and 80% completion, where $C_{15}COOH$ and $C_{16}COOH$ are the respective monocarboxylic acids (i.e., SA is $C_{17}COOH$). Ziemann[19] also reports that the reaction kinetics of oleic acid loss show a rapid reaction regime followed by a slower rate of loss. Hearn and Smith[42] report that the loss rate of oleic acid

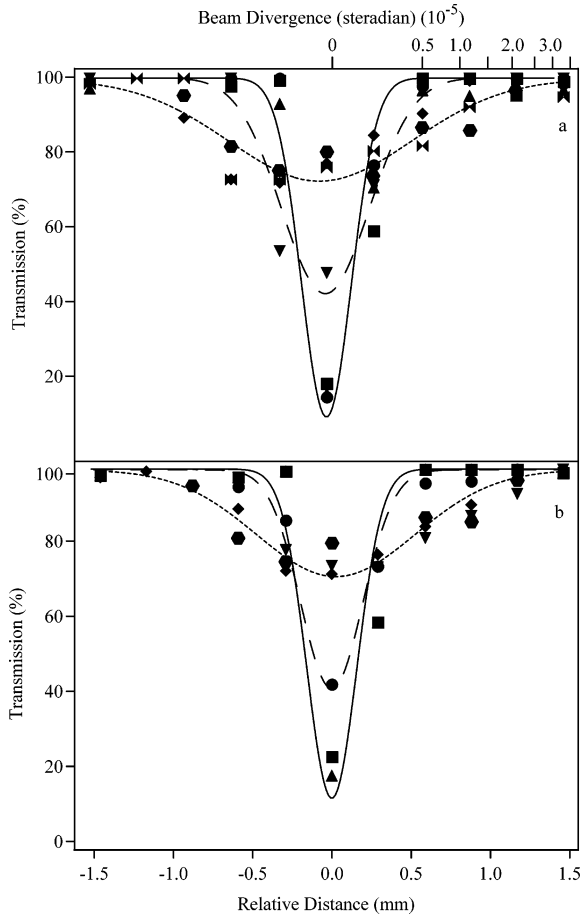

Figure 5. (a) Beam profiles of unreacted particles. (b) Beam profiles of particles reacted for 300×10^{-6} atm·s·O_3. The integrated mass spectrum is employed for signal strength in calculating the beam profile. Lines are discussed in the text. For comparison, 130-nm vacuum aerodynamic diameter aqueous NaCl particles have a beam width of 0.4×10^{-5} steradian (i.e., the same as the solid lines in Figure 5) while their cubic crystalline counterparts have a beam width of 1.6×10^{-5} steradian.[26] See key and further details about reaction conditions in the captions of Figures 3 and 4.

slows by a factor of 12 in the reaction of 25/75 OL/$C_{13}COOH$ provided that the particles are prepared with $C_{13}COOH$ in its solid phase. Although different particle sizes, ozone concentrations, reaction times, and matrix chemistries should be taken into account,[24] these recent results in the literature are remarkably consistent with those of this study for mixed OL/SA particles.

As shown in Figure 2, the presence of stearic acid in the particle can lead to formation of a solid that strongly distorts the particle from a spherical shape. The divergence of the particle beam inside the AMS provides a complementary probe of the aerosol particle shape in situ.[26] The beam profiles of unreacted and reacted particles are shown in Figure 5 (300×10^{-6} atm·s of ozone exposure). The seven beam profiles in Figure 5 can be characterized by three Gaussian fits: one fit (solid line) for well-focused particles characteristic of spheres; one fit (dashed line) for less focused particles; and one fit (double-dashed line) for defocused particles characteristic of irregularly shaped solids. For unreacted particles, the respective three groupings are 100/0, 90/10, and 75/25; 60/40; and 50/50, 30/70, and 10/90. For reacted particles, the respective three grouping are 100/0 and 90/10; 75/25; and 60/40, 50/50, 30/70, and 10/90. Therefore, the 75/25 and 60/40 particles change shape upon chemical reaction. Particles having an SA content greater than 60/40 may also change shape, but the change may go

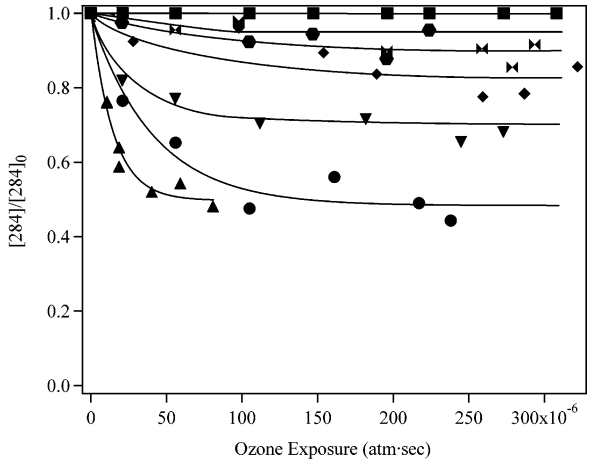

Figure 6. Decay of the molecular peak of stearic acid ($[284]/[284]_0$) for increasing ozone exposure. Key: 90/10 OL/SA (▲); 75/25 OL/SA (●); 60/40 OL/SA (▼); 50/50 OL/SA (◆); 30/70 OL/SA (⋈); 10/90 OL/SA (⬣); 0/100 OL/SA (■). Lines are to guide the eye and do not represent a model fit. Data for Figures 4 and 6 are recorded contemporaneously. See further details about reaction conditions in the caption of Figure 3.

undetected: given their initial irregular shape, the divergence of the particle beam may be little changed by alterations in shape.

Figure 6 shows that the amount of stearic acid in the particles decreases with increasing ozone exposure. Due to the absence of a double bond in its chemical structure, stearic acid does not react directly with ozone. Rather, the stabilized Criegee intermediate (SCI) formed by oleic acid ozonolysis attacks the carboxylic acid group of stearic acid to yield an α-acyloxyalkyl hydroperoxide product.[18,19,24,28] Therefore, the kinetic behavior of stearic acid is closely driven by the observations seen in Figure 4 for oleic acid: the characteristic decay parameter is nearly identical in Figures 4 and 6 for the 90/10, 75/25, and 60/40 OL/SA particles. The kinetic behavior for particles of 50/50 and greater SA content, however, is different between Figures 4 and 6. Moreover, Figure 6 shows that the percent loss of SA decreases as the OL content of the particle decreases, as expected since oleic acid is the source of the SCI reactant.

An approximate branching ratio of the SCI reaction with SA versus other pathways (i.e., those active in pure oleic acid[24]) can be estimated. For example, given that one SCI is produced from each OL molecule, the SCI + SA channel is the sink for approximately 5.5% of the generated SCI in 90/10 OL/SA particles. This value is calculated as the quotient of 5 divided by 90 by noting that, in a hypothetical 100-mol particle (molecular weights of 282 and 284 g mol^{-1} for OL and SA, respectively), a 50% loss of SA (cf. loss of SA in Figure 6) corresponds to 5 mol of SA while 90 mol of SCI is generated (cf. complete loss of OL in Figure 5). Similarly, the channel accounts for 18% (i.e., [(0.5)(25)]/[(0.95)(75)] using information in Figures 4 and 6) of the SCI loss for 75/25 OL/SA particles, 24% for 60/40 OL/SA particles, and up to 64% for 10/90 OL/SA particles. The importance of the SCI + SA pathway as a scavenger of SCI, therefore, increases for increasing SA content, as expected.

4. Discussion

4.1. Reactive Uptake Coefficients. An uptake coefficient (γ) is a convenient overall parameter for quantitatively representing the combined effects of various physical processes that determine the rate of a heterogeneous reaction of a gas-phase species such as ozone with a condensed-phase species such as oleic acid.[51] The uptake coefficient is the fractional net loss of the gas-phase species compared to the gas-phase collision rate. Physical processes affecting the fractional net loss include the accommodation fraction at the surface, Henry's law solubility, the diffusion of dissolved species in the condensed phase, and the rates of chemical reactions. The uptake coefficient therefore varies in time as the dominant governing process changes. For example, initially, the uptake can be rapid until Henry's law solubility limit is reached in the surface region. Subsequently, the uptake may slow as condensed-phase diffusion limits overall gas uptake. In all cases, after an initial transient period, which is effectively instantaneous for typical laboratory kinetic setups, the slowest step in the train of processes depends on the rate of chemical reaction and, in this time regime, the so-called reactive uptake coefficient governs. The rate of chemical reaction can be governed by chemical factors such as bimolecular rate constants and by physical factors such as diffusion coefficients.

In models of heterogeneous gas−liquid chemistry, limiting cases for the rate of chemical reaction can be described,[14,51,52] for which the rate-limiting process governing the reactive uptake coefficient may be one of slow gas-phase diffusion of the reactant, slow accommodation of the gas-phase reactant at the surface (implying that the chemical reaction is then localized at the surface), rapid reaction in the surface region compared to slow reaction in the bulk (i.e., different rate constants in the different chemical environments), slow diffusion of the dissolved gas-phase reactant into the particle (implying that the chemical reaction could be faster if the reactant could mix more rapidly), or slow diffusion of the condensed-phase reactant into the reaction zone (implying a gradient in the concentration of this species along the radial axis). For each of these cases, mathematical forms have been developed, and the successful fit of a kinetic data set to one of the mathematical forms is taken as evidence to support that one of the limiting cases is active and also to obtain a reactive uptake coefficient from the fit parameters.[18]

In applications to ozonolysis of pure oleic acid, the results have been ambiguous in that two of the mathematical models appear to fit the data, namely that of a localized surface reaction and that of slow diffusion of the dissolved gas-phase reactant. Therefore, in the literature on oleic acid ozonolysis, there is controversy[18,20] whether the reaction occurs at the interface[18] or in the bulk medium.[12,14,16,19,53] The two fits are equally successful perhaps because the reactive parameters such as the diffusion coefficients or Henry's law parameters change as the reaction medium itself is substantially altered from the initial oleic acid environment. For pure oleic acid particles, there is typically no oleic acid remaining at the end of the reaction, having been replaced by a range of organic products.

These complications also hold for experiments with mixed particles, in which the final chemical composition of the particle after ozone exposure is very different from the original. Moreover, the validity of the application of these model equations to particles of mixed composition,[20] especially those containing some portion of solid stearic acid in an uncertain morphological arrangement, is untested. Instead of these model-driven approaches, in this study, we therefore use a data-driven approach, as follows.

The net fraction of particle−surface collisions of ozone molecules resulting in the loss of ozone (i.e., the uptake coefficient) can be estimated for a single particle of surface area A and volume V. The number of ozone molecules passing through a unit surface area per unit time (e.g., impacting a

particle surface) is given by gas kinetic theory as $P\bar{c}/4RT$, where P is the partial pressure of O_3, $\bar{c}$ is the mean speed of O_3 molecules in gas-phase N_2 (360 m s^{-1}), R is the gas constant, and T is the temperature.

Two assumptions are made for the further development of the data-driven approach. (1) The concentration profile of dissolved ozone inside the particle is at steady state so that any further ozone uptake by the particles arises from chemical reaction. (2) A surrogate for the chemical reaction rate of ozone is the chemical reaction rate of its ozonolysis partner, in this case oleic acid. Therefore, under this assumption, monitoring the reaction rate of oleic acid in a particle (d[OL]/dt) is equivalent to measuring the volume-averaged loss rate of ozone in the particle, where [OL] is the oleic acid concentration (mol L^{-1}). The second assumption is not fully accurate because the ozonolysis products of oleic acid form reactive stabilized Criegee intermediates that can also react with oleic acid,[18,19,22,23] thereby amplifying the reactive impact of a single ozone molecule. One estimate is that the amplification factor is 36%,[18] although the exact amplification depends on the reaction conditions. An example of this dependence is discussed in connection with Figure 6 for which the SCI + SA channel increases from approximately 6% of the generated SCI for 90/10 particles to 64% for 10/90 particles. The SCI + OL channel is then inferred as becoming a less important amplification pathway for increasing SA content.

An oleic acid loss rate of d[OL]/dt inside the particle of volume V and surface area A corresponds to a unit-surface-area loss rate of (d[OL]/dt)(V/A). Therefore, the net fraction of particle−surface collisions of ozone molecules resulting in the loss of ozone because of chemical reaction (i.e., the reactive uptake coefficient γ) is given as

$$\gamma = \frac{(-\mathrm{d[OL]}/\mathrm{d}t)(V/A)}{P\bar{c}/4RT} \qquad (1)$$

For a homogeneous spherical particle, the geometric factor (V/A) is $D/6$, where D is the particle diameter. Equation 1 provides an upper limit for γ because (a) the unit-surface-area ozone consumption rate is assumed to equal the unit-surface-area loss rate of oleic acid, which, given that the latter is greater than the former as discussed for assumption no. 2, implies an upper limit for γ calculated by eq 1 and (b) any nonspherical particle, such as those indicated by the beam probe experiment and suggested by the TEM micrographs, has a lower V/A than the spherical particle we assume in evaluation of eq 1, thus implying γ is an upper limit.

The aerosol mass spectrometer measures the mass of a particle population. The aerosol mass of oleic acid particles is denoted m_{OL}. For a monodisperse aerosol, such as employed in this study, m_{OL} and [OL] are related by $m_{OL} = N[\mathrm{OL}]VM_{W,OL}$, where N is the number concentration of the aerosol particles and $M_{W,OL}$ is the relative molecular mass of oleic acid. The resulting equation is as follows:

$$\gamma = \frac{-\mathrm{d}m_{OL}/\mathrm{d}t}{(P\bar{c}/4RT)(M_{W,OL}NA)} \qquad (2)$$

(Kinetic treatments can also be adapted to a polydisperse distribution.[17])

The loss rates d[OL]/dt and hence d[m_{OL}]/dt slow with decreasing [OL] because the underlying rate law is bimolecular and therefore the loss rate is proportional to [O_3][OL]. As a result, because [OL] decreases with time, γ also decreases. For this reason, the convention is to extrapolate data to zero time

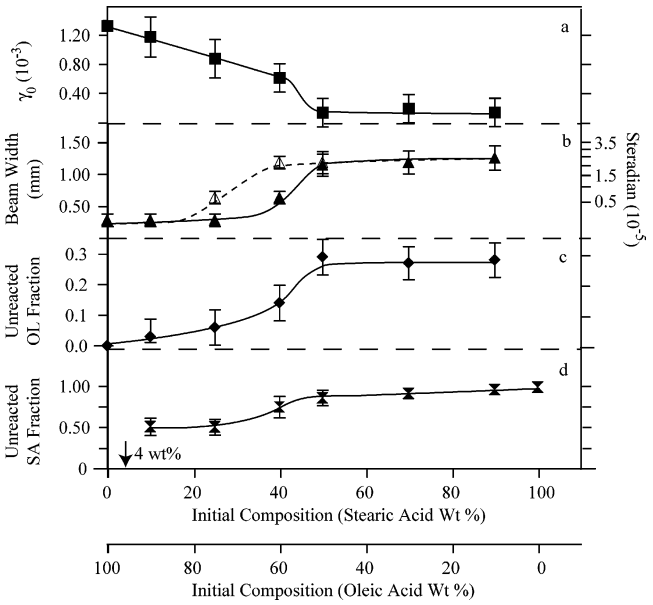

Figure 7. Summary of results for increasing stearic acid composition: (a) initial reactive uptake coefficient (γ_0) (eq 2); (b) beam width before (▲) and after (△) ozone exposure (300×10^{-6} atm·s·O_3); (c) unreacted oleic acid fraction after ozone exposure; (d) unreacted stearic acid fraction after ozone exposure. Quantities are shown for increasing stearic acid weight percent composition, with the balance of the composition being oleic acid. Lines are to guide the eye and do not represent a model fit. The arrow at 4 wt % indicates the composition of a liquid in equilibrium with pure, solid stearic acid at 298 K.[41] See further details about reaction conditions in the caption of Figure 3.

to calculate an initial reactive uptake coefficient γ_0 (i.e., the uptake when [OL] is at its initial value).

As a practical matter, in our experimental approach, for a given OL/SA composition we fix time at 7 s and vary P. We observe the drop of m_{OL} in 7 s, thus measuring Δm_{OL}/7 s as an approximation to dm_{OL}/dt. For example, for the data shown in Figure 4, $\Delta m_{OL}(P)/7\ \mathrm{s} = m_{OL}(P \times 0\ \mathrm{s})[1 - m_{OL}(P \times 7\ \mathrm{s})/m_{OL}(P \times 0\ \mathrm{s})]/(7\ \mathrm{s})$. Evaluation of eq 2 at one P for one OL/SA composition using a surface area calculated as πD^2 with $D = 300$ nm yields one estimate of γ_0 (which is an upper limit for the reasons discussed in relation to eq 1). We repeat this calculation for all P we have satisfying $m_{OL}(P \times 7\ \mathrm{s})/m_{OL}(P \times 0\ \mathrm{s}) > 0.6$ so as to stay in the regime of initial reactive uptake. The average of these several estimates of γ_0 is reported for that OL/SA composition. We repeat this process for each OL/SA composition. The reported γ_0(OL/SA) values are upper limits because of the uncertainties of amplification discussed above regarding assumption no. 2.

As a result of this analysis, we find that γ_0 of 100/0 OL/SA particles is $1.25\ (\pm 0.2) \times 10^{-3}$. This result is in good agreement with other aerosol studies (e.g., see summary of eight studies in Table 1 of Knopf et al.[20]). Our analysis finds that γ_0 decreases linearly from 100/0 to 60/40 from $1.25\ (\pm 0.2) \times 10^{-3}$ to $0.60\ (\pm 0.15) \times 10^{-3}$ (Figure 7). At 50/50, there is an abrupt drop in γ_0 to $0.15\ (\pm 0.1) \times 10^{-3}$, and within experimental uncertainty, γ_0 apparently undergoes no further changes from 50/50 to 10/90. In the only other report to our knowledge of γ_0 for oleic-acid mixed particles, Ziemann reports that γ_0 is $0.06\ (\pm 0.2) \times 10^{-3}$ and $0.15\ (\pm 0.5) \times 10^{-3}$ for 10/90 particles of OL/C_{15}-COOH and OL/C_{16}COOH, respectively, where C_{17}COOH is SA.

Knopf et al.[20] study films of OL/C_{11}COOH and OL/C_{13}COOH from 100/0 to 0/100 composition in steady increments. In a trend similar to our results, monitoring ozone loss, these authors report that γ_0 of ozone uptake (i.e., not γ_0 of oleic acid loss) decreases

linearly as the alkanoic acid content increases, at least until a critical composition above which γ_0 abruptly drops by a factor of 10 or more depending on how the film is prepared. The authors attribute the abrupt drop in γ_0 to partial solid formation in the film and suggest that the dependence of γ_0 on the method of film preparation is related to different solid−liquid dendritic microstructures in the film that affect the relative chemical availability of oleic acid. The critical film composition for the abrupt drop in γ_0 is approximately the same as indicated by the liquidus line (i.e., solid formation) in the phase diagrams of the binary OL/C_{11}COOH and OL/C_{13}COOH systems. In comparison, we observe an abrupt drop only between 40 and 50 wt % oleic acid in the OL/SA system, whereas the phase diagram indicates solid formation at 4 wt %.[41]

4.2. Chemical Morphology. The results of this study are summarized in Figure 7. Three composition regions, namely 100/0 to 60/40, 60/40 to 50/50, and 50/50 to 0/100, are apparent in the behavior of the initial reactive uptake coefficient, the particle beam width, the unreacted oleic acid fraction at high ozone exposure, and the unreacted stearic acid fraction at high ozone exposure. In the first composition region, linear trends in these parameters are observed for increasing SA composition. In the second composition region, there is an abrupt change in all parameters. In the third composition region, the parameters either do not change further within experimental sensitivity or change only slightly for increasing SA composition.

The trends in Figure 7 can be explained by invoking three reasonable postulates of chemical morphology: (1) Particles remain liquid beyond the liquidus composition (i.e., supersaturation). (2) The stearic acid solid holds a large quantity of oleic acid as an impurity inside its crystal structure when it crystallizes. (3) Accompanying crystallization, some stearic acid molecules connect as a filamentous network to form a semipermeable gel containing liquid OL. The ordinal ranking of the uptake coefficients of OL in these three chemical morphologies is $\gamma^{(1)} > \gamma^{(3)} \gg \gamma^{(2)}$.

The first postulate can be justified by the fact that submicron particles regularly support high supersaturations in the absence of heterogeneous nuclei because homogeneous nucleation is slow in small volumes.[54] Hearn and Smith show that 13/87 OL/C_{13}COOH particles prepared by cooling of hot vapors are able to supercool by at least 32 K (i.e., they do not form solid C_{13}-COOH).[42] In contrast, Knopf et al. show that films of OL/C_{11}-COOH and OL/C_{13}COOH form solids precisely at compositions predicted by the phase diagram. These differences in supercooling behavior between submicron particles and films arise because film volumes are much larger than those of particles and because films are in contact with a heterogeneous nucleus of a glass wall.

The first postulate is necessary to explain the experimental observations because particles of OL/SA have an exoergic driving force for crystallization for compositions with an SA content greater than 96/4 whereas the data in Figure 7 suggest that the particles crystallize only between 60/40 and 50/50, corresponding to 30 to 33 K of supercooling at 298 K by the phase diagram of Inoue et al.[41] Therefore, we conclude that submicron particles of OL/SA prepared by atomization and evaporation of methanol at 298 K are able to significantly supersaturate.

The second postulate is reasonable because rapidly growing crystals, such as occurs for SA crystals inside the particles when methanol evaporates, can incorporate large amounts of impurities.[55,56] In particular, Inoue et al.[57] suggest that OL/C_{11}COOH, OL/C_{13}COOH, and OL/C_{15}COOH crystallize with high levels of oleic acid impurity when 5 to 10 mg mixtures are cooled by 2 to 3 K min^{-1} to 243 K. Although the results of Inoue et al. also indicate that stearic acid mixed with oleic acid (i.e., OL/C_{17}COOH) behaves differently by crystallizing as pure separate phases at 243 K, the behavior of crystallization at 298 K and in submicron particles is not investigated, and these may be important differences. Therefore, we feel that the observations of Inoue et al. provide support to the postulate that SA crystals incorporate large amounts of OL impurities as methanol evaporates from the submicron particles.

The second postulate is necessary to explain the large fraction of unreacted oleic acid in OL/SA particles having SA solids. The corollary to this postulate is that OL acid inside the SA crystals is essentially unavailable for reaction with O_3 because it is locked in the solid lattice. The purities of the SA crystals can be estimated from the data summarized in Figure 7c,d. For example, after reaction, an initial 75/25 particle has remaining 5% of its OL and 50% of its SA. Therefore, the SA crystal has a purity of approximately 77 wt %. This number is calculated by noting that, after reaction, a hypothetical 100-g particle has 3.75 g of OL (calculated as 5% of 75 g) and 12.5 g of SA remaining. The calculation omits the possible role of any product species. Similar calculations give approximately 76 wt % SA purity for particles initially of 60/40, 74 wt % for 50/50, 88 wt % for 30/70, and 97 wt % for 10/90. These results could suggest a maximum impurity level of 25 wt % OL in SA for compositions of 75/25 through 50/50. Furthermore, the results show a decreasing impurity level for lower initial OL concentrations, as expected, from 50/50 to 10/90.

The second postulate could also explain the behavior observed by Ziemann[19] that oleic acid first reacts quickly and then more slowly by orders of magnitude. Namely, liquid oleic acid reacts first and accounts for the first reaction stage. We hypothesize that the stearic acid in individual particles recrystallizes according to the stochastic processes of homogeneous nucleation and that the slow reaction stage is a monitor of these phase changes. As each individual particle recrystallizes, the oleic acid is released from the matrix and is available for ozonolysis. We are not able to probe this slow-stage behavior in our experiment because the reaction time is fixed at 7 s whereas Ziemann observe this phenomenon across 480 s. According to this explanation, as a proposed thought experiment, during the time period of 480 s a single-particle mass spectrometer should detect an externally mixed aerosol, consisting of some particles that will have recrystallized (negligible residual OL content) and others that will have not (high OL content).

The third postulate is reasonable because the preferential habit of stearic acid as needles (cf. Figure 2) suggests that a filamentous molecular network forms prior to full crystallization. The network is supported by interstitial oleic acid. This structure is a semipermeable gel of low diffusivity for oleic acid and ozone, thus reducing γ_0.

A gel phase inside the particles is different from the dendrites proposed by Knopf et al.[20] for films. A gel is based upon molecular filaments whereas dendrites are solids of submicrometer dimensions. A gel, however, may be a molecular precursor to dendrite growth in a film. A minimum system dimension of at least 500 nm and possibly up to 2 μm is necessary for the development of coupled diffusion and growth that give rise to dendrites.[58] The physics of dendrite growth, therefore, are applicable to films but not to accumulation-mode (i.e., submicron) atmospheric particles.

The third postulate is necessary to explain the decrease in γ_0 from 1.25 ($\pm$0.2) $\times$ 10^{-3} for pure oleic acid to 0.13 ($\pm$0.1) $\times$

10^{-3} for compositions from 50/50 to 10/90 (Figure 7a), as follows. The aerosol particles are irregularly shaped (Figures 7b), which implies that they contain a solid phase. The phase diagram[41] of OL/SA shows that the liquid-phase composition is 96 wt % OL at 298 K. The liquidus chemical composition is a fixed thermodynamic quantity from 50/50 to 10/90; therefore, γ_0 should not change across this range. In agreement with this prediction, within experimental uncertainty γ_0 does not change from 50/50 to 10/90 (Figure 7a), although there may be changes that we cannot detect because of shifts in the amplification factor or in the *V/A* ratio from 50/50 to 10/90 (cf. discussion surrounding eq 1). A further constraint is that γ_0 from 50/50 to 10/90 (i.e., 96 wt % oleic acid liquid phase according to the phase diagram) should be nearly equal to γ_0 of 100/0. The data, however, show a large decrease in γ_0 for 50/50 through 10/90 compared to the value at 100/0. A postulate must be invoked, in this case that of a gel, to reduce the uptake coefficient.

As a general statement, all other factors being equal, the phase change from a supercooled/supersaturated state to an equilibrium composition should increase the oleic acid enrichment of the reactive liquid phase and therefore the uptake coefficient. On the contrary, the data in Figure 7a show that γ_0 drops by more than a factor of 10 when solidification occurs (i.e., γ_0 of 50/50 to 10/90 compared to that of 100/0). In an elegant experiment, Hearn and Smith[42] explicitly demonstrate that solidification of OL/C_{13}COOH particles decreases the reaction rate by a factor of 12. Ziemann shows that 10/90 OL/C_{15}COOH and OL/C_{16}COOH particles react 5−10 times more slowly than pure oleic acid particles, although the liquid-phase composition inferred from the phase diagram alone would suggest much smaller reductions. Therefore, an additional explanation must be invoked to explain our results, those of Hearn and Smith,[42] and those of Ziemann,[19] all of which clearly show that γ_0 decreases upon solidification of particles. These observations all motivate the third postulate that a gel phase forms that reduces the diffusivity of reactants and hence the uptake coefficient.

The gel is believed to reduce the diffusion coefficient of both ozone and oleic acid. In the ozonolysis of pure particles of oleic acid, the diffusion of ozone is rate-limiting in comparison to that of oleic acid, which is thoroughly mixed at all times. The implication is that although the diffusion processes of ozone and oleic acid are slowed in the gel, the reduction in the diffusion coefficient of ozone is the important feature leading to the decreased uptake coefficient.

The results summarized in Figure 7 for mixed OL/SA particles can be interpreted with the guidance of these three postulates. Prior to ozonolyis, particles from 90/10 to 60/40 are supersaturated liquids and spherical (Figure 7b). The initial uptake coefficient is proportional to the oleic acid concentration in the liquid phase[12,52] and therefore decreases as the SA composition increases (Figure 7a). During the course of the reaction, oleic acid reacts, nonanal evaporates, and the stearic acid wt % composition increases. As a result, for 75/25 and 60/40, stearic acid crystallizes: the particles lose their spherical shape (Figure 7b) and the imperfect crystal of stearic acid holds oleic acid so that the reaction is incomplete (Figure 7c).

The behavior shown in Figure 7 for particles from 50/50 to 10/90 can also be interpreted with the guidance of the above postulates. The beam width in Figure 7b shows that the aerosol particles in situ contain a solid phase large enough to perturb them aerodynamically. The solid phase, according to the second postulate, is stearic acid having a large impurity of oleic acid that isolates it from reaction with ozone and thus leaves a high fraction of unreacted oleic acid (Figure 7c). The solid phase may be the monolithic needles apparent in Figure 2, although recrystallization may take place during the several days that pass between particle collection and imaging. According to the third postulate, a gel phase of filamentous stearic acid and interstitial oleic acid partially envelopes the solid phase. This gel reduces γ_0 (Figure 7a) and also presents a fraction of the stearic acid to attack by stabilized Criegee intermediates, thus reducing the SA content in the particles after reaction (Figure 7d). The gel partially, rather than completely, envelopes the solid because the results of the beam probe show that the particles are irregularly shaped. In this regard, the images in Figure 2 provide appropriate possible examples of partially enveloped needles.

4.3. Conclusions. The results of this study show that the chemical environment surrounding an organic molecule dramatically alters its rates of chemical reaction. In particular, the results highlight the importance of particle phase and also chemical morphology within the particle: oleic acid in liquid regions of a particle reacts rapidly with ozone whereas oleic acid trapped inside solid stearic acid is essentially unavailable for reaction with ozone, at least on the time scale of our experimental measurements. These findings, therefore, provide a plausible explanation for reconciling, on one hand, observations of an atmospheric lifetime of days to weeks for condensed-phase oleic acid with, on the other hand, the implications of earlier laboratory studies that liquid-phase oleic acid should be present for at most several minutes in typical polluted urban environments of 100 ppb O_3.

Although stearic acid and oleic acid are common constituents of atmospheric particles in urban areas that cook large amounts of meat, mixed oleic-acid/stearic-acid particles are still a gross simplification of atmospheric particles. Primary and secondary organic aerosol particles are composed of hundreds if not thousands of organic molecules. Theoretical studies suggest that liquid phases may dominate under these conditions,[59] although laboratory and field studies concerning the presence and the absence of solid organic phases have not yet been carried out. These uncertainties noted, we assume for purposes of discussion that the mixed oleic-acid/stearic-acid particles we have studied serve as a proxy of the broader class of heterogeneous oxidation chemistry relevant to real atmospheric particles.

The implications of the results of this study for source apportionment in urban airsheds could be that the portion of particulate-matter oleic acid in the liquid phase reacts quickly while the portion trapped in the solid phase remains inert. This second fraction would be detected by analysis and employed in quantitative source apportionment. As a result, because oleic acid is employed to apportion the contribution of meat cooking activities to urban particulate matter and because the detected oleic acid would be less than that emitted due to ozonolysis of the liquid fraction, meat smoking activities would be negatively biased in the apportionment assessment.

The results reported in this paper contribute to the continuing development of the scientific community's understanding of particle aging process in the atmosphere, for which the ultimate goal is to provide quantitative mechanistic models of physicochemical transformations under atmospheric conditions. At present, state-of-the-art global models[11,60−64] use a simplified treatment by imposing a conversion lifetime of 1−2 days[65] from hydrophobic to hydrophilic particle classes, regardless of the nature of the carbon or the presence or the absence of gas-phase oxidants such as ozone or hydroxyl radical. The rationale for this simplification arises, at least in part, because of

computational simplicity, because of incomplete source characterizations, and because of limited understanding of the physics and the chemistry. The results of this and other laboratory studies are beginning to address this last point.

Understanding and predicting the changes in the physicochemical properties of atmospheric particles during aging by oxidation should lead to several important improvements in understanding and therefore addressing atmospheric problems. Principally, the oxidation of organic matter can lead to greater hygroscopicity.[66−70] Consequently, aging can change particles from CCN-inactive to CCN-active, thus potentially affecting cloud formation.[71,72] Further changes in the hydrological cycle and global and regional climate may result.[5,8,73,74] In addition, changes in the chemical species and the hygroscopic properties of airborne particulate matter influence the human health effects of inhaled particulate matter and the magnitude of visibility pollution in urban areas and national parks.

Acknowledgment. This material is based upon work supported by the National Science Foundation under Grant No. ATM-0215357. Any opinions, findings, and conclusions or recommendations expressed in this material are those of the authors and do not necessarily reflect the views of the National Science Foundation.

References and Notes

(1) Seinfeld, J. *National Research Council, Panel on Aerosol Radiative Forcing and Climate Change. A Plan for a research program on aerosol radiative forcing and climate change*; National Academy Press: Washington, DC, 1996.

(2) Heintzenberg, J. *Chem. Unserer Zeit.* **1999**, *33*, 158−164.

(3) Haywood, J.; Boucher, O. *Rev. Geophys.* **2000**, *38*, 513−543.

(4) Ramaswamy, V.; Boucher, O.; Haigh, J.; Hauglustaine, D.; Haywood, J. M.; Myhre, G.; Nakajima, T.; Shi, G. Y.; Solomon, S. Radiative forcing of Climate Change. In *Climate Change 2001: The Scientific Basis. Contribution of Working Group I to the Third Assessment Report of the Intergovernmental Panel on Climate Change*; Houghton, J. T., Ding, Y., Griggs, D. J., Noguer, M., Linden, P. v. d., Dai, X., Maskell, K., Eds.; Cambridge University Press: New York, 2001; pp 349−416.

(5) Ramanathan, V.; Crutzen, P. J.; Kiehl, J. T.; Rosenfeld, D. *Science* **2001**, *294*, 2119−2124.

(6) Samet, J. *Research Priorities for Airborne Particular Matter. 1. Immediate Priorities and a Long-Range Research Porfolio*; National Academy Press: Washington, DC, 1998.

(7) Ellison, G. B.; Tuck, A. F.; Vaida, V. *J. Geophys. Res.* **1999**, *104*, 11633−11641.

(8) Jacobson, M. C.; Hansson, H. C.; Noone, K. J.; Charlson, R. J. *Rev. Geophys.* **2000**, *38*, 267−294.

(9) Rudich, Y. *Chem. Rev.* **2003**, *103*, 5097−5124.

(10) Seinfeld, J. H.; Pankow, J. F. *Annu. Rev. Phys. Chem.* **2003**, *54*, 121−140.

(11) Kanakidou, M.; Seinfeld, J. H.; Pandis, S. N.; Barnes, I.; Dentener, F. J.; Facchini, M. C.; Van Dingenen, R.; Ervens, B.; Nenes, A.; Nielsen, C. J.; Swietlicki, E.; Putaud, J. P.; Balkanski, Y.; Fuzzi, S.; Horth, J.; Moortgat, G. K.; Winterhalter, R.; Myhre, C. E. L.; Tsigaridis, K.; Vignati, E.; Stephanou, E. G.; Wilson, J. *Atmos. Chem. Phys.* **2005**, *5*, 1053−1123.

(12) Morris, J. W.; Davidovits, P.; Jayne, J. T.; Jiménez, J. L.; Shi, Q.; Kolb, C. E.; Worsnop, D. R.; Barney, W. S.; Cass, G. *Geophys. Res. Lett.* **2002**, *29*, 1357.

(13) Moise, T.; Rudich, Y. *J. Phys. Chem. A* **2002**, *106*, 6469−6476.

(14) Smith, G. D.; Woods, I. E.; DeForest, C. L.; Baer, T.; Miller, R. E. *J. Phys. Chem. A* **2002**, *106*, 8085−8095.

(15) Smith, G. D.; Woods, E.; Baer, T.; Miller, R. E. *J. Phys. Chem. A* **2003**, *107*, 9582−9587.

(16) Thornberry, T.; Abbatt, J. P. D. *Phys. Chem. Chem. Phys.* **2004**, *6*, 84−93.

(17) Hearn, J. D.; Smith, G. D. *J. Phys. Chem. A* **2004**, *108*, 10019−10029.

(18) Hearn, J. D.; Lovett, A. J.; Smith, G. D. *Phys. Chem. Chem. Phys.* **2005**, *7*, 501−511.

(19) Ziemann, P. J. *Faraday Discuss.* **2005**, *130*, 469−490.

(20) Knopf, D. A.; Anthony, L. M.; Bertram, A. K. *J. Phys. Chem. A* **2005**, *109*, 5579−5589.

(21) Rebrovic, L. *J. Am. Oil Chem. Soc.* **1992**, *69*, 159−165.

(22) Katrib, Y.; Martin, S. T.; Hung, H. M.; Rudich, Y.; Zhang, H.; Slowik, J. G.; Davidovits, P.; Jayne, J. T.; Worsnop, D. R. *J. Phys. Chem. A* **2004**, *108*, 6686−6695.

(23) Zahardis, J.; LaFranchi, B. W.; Petrucci, G. A. *J. Geophys. Res.* **2005**, *110*, D08307.

(24) Hung, H. M.; Katrib, Y.; Martin, S. T. *J. Phys. Chem. A* **2005**, *109*, 4517−4530.

(25) Asad, A.; Mmereki, B. T.; Donaldson, D. J. *Atmos. Chem. Phys.* **2004**, *4*, 2083−2089.

(26) Katrib, Y.; Martin, S. T.; Rudich, Y.; Davidovits, P.; Jayne, J. T.; Worsnop, D. R. *Atmos. Chem. Phys.* **2005**, *5*, 275−291.

(27) Broekhuizen, K. E.; Thornberry, T.; Kumar, P. P.; Abbatt, J. P. D. *J. Geophys. Res.* **2004**, *109*, D24206.

(28) Bailey, P. S. Ozonation in Organic Chemistry. In *Organic Chemistry*; Trahanovsky, W., Ed.; Academic Press: London, 1978; Vol. I, Olefinic Compounds.

(29) Gill, P. S.; Graedel, T. E.; Weschler, C. J. *Rev. Geophys. Space Phys.* **1983**, *21*, 903−920.

(30) Rogge, W. F.; Hildemann, L. M.; Mazurek, M. A.; Cass, G. R.; Simonelt, B. R. T. *Environ. Sci. Technol.* **1991**, *25*, 1112−1125.

(31) Stephanou, E. G.; Stratigakis, N. *Environ. Sci. Technol.* **1993**, *27*, 1403−1407.

(32) Schauer, J. J.; Rogge, W. F.; Hildemann, L. M.; Mazurek, M. A.; Cass, G. R. *Atmos. Environ.* **1996**, *30*, 3837−3855.

(33) Gurr, M. I.; Harwood, J. L.; Frayn, K. N. *Lipid Biochemistry*; Iowa State Press: Iowa City, IA, 2002.

(34) Vance, D. E.; Vance, J. E. *Biochemistry of Lipids, Lipoproteins and Membranes*; Elsevier: Amsterdam, 2002.

(35) Rogge, W. F.; Mazurek, M. A.; Hildemann, L. M.; Cass, G. R.; Simoneit, B. R. T. *Atmos. Environ.* **1993**, *27A*, 1309−1330.

(36) Hildemann, L. M.; Mazurek, M. A.; Cass, G. R.; Simoneit, B. R. T. *Environ. Sci. Technol.* **1991**, *25*, 1311−1325.

(37) Hamilton, J. F.; Webb, P. J.; Lewis, A. C.; Hopkins, J. R.; Smith, S.; Davy, P. *Atmos. Chem. Phys.* **2004**, *4*, 1279−1290.

(38) Iwahashi, M.; Kasahara, Y.; Matsuzawa, H.; Yagi, K.; Nomura, K.; Terauchi, H.; Ozaki, Y.; Suzuki, M. *J. Phys. Chem. B* **2000**, *104*, 6186−6194.

(39) Iwahashi, M.; Suzuki, M.; Czarnecki, M. A.; Liu, Y. L.; Ozaki, Y. *J. Chem. Soc., Faraday Trans.* **1995**, *91*, 697−701.

(40) Iwahashi, M.; Yamaguchi, Y.; Kato, T.; Horiuchi, T.; Sakurai, I.; Suzuki, M. *J. Phys. Chem.* **1991**, *95*, 445−451.

(41) Inoue, T.; Hisatsugu, Y.; Yamamoto, R.; Suzuki, M. *Chem. Phys. Lipids* **2004**, *127*, 143−152.

(42) Hearn, J. D.; Smith, G. D. *Phys. Chem. Chem. Phys.* **2005**, *7*, 2549−2551.

(43) Knutson, E. O.; Whitby, K. T. *J. Aerosol Sci.* **1975**, *6*, 443−451.

(44) Jayne, J. T.; Leard, D. C.; Zhang, X.; Davidovits, P.; Smith, K. A.; Kolb, C. E.; Worsnop, D. R. *Aerosol. Sci. Technol.* **2000**, *33*, 49−70.

(45) Jimenez, J. L.; Jayne, J. T.; Shi, Q.; Kolb, C. E.; Worsnop, D. R.; Yourshaw, I.; Seinfeld, J. H.; Flagan, R. C.; Zhang, X. F.; Smith, K. A.; Morris, J. W.; Davidovits, P. *J. Geophys. Res.* **2003**, *108*, 8425.

(46) Huffman, J. A.; Jayne, J. T.; Drewnick, F.; Aiken, A. C.; Onasch, T.; Worsnop, D. R.; Jimenez, J. L. Submitted for publication.

(47) Zhang, X.; Smith, K. A.; Worsnop, D. R.; Jimenez, J. L.; Jayne, J. T.; Kolb, C. E.; Morris, J.; Davidovits, P. *Aerosol Sci. Technol.* **2004**, *38*, 619−639.

(48) Agarwal, J. K.; Sem, G. J. *J. Aerosol Sci.* **1980**, *11*, 343−357.

(49) Rader, D. J. *Application of the Tandem Differential Mobility Analyzer to the Studies of Droplet Evaporation and Growth*; University of Minnesota: Minneapolis, MN, 1985.

(50) Hinds, W. C. *Aerosol Technology: Properties, Behavior, and Measurement of Airborne Particles*; Wiley: New York, 1999.

(51) Kolb, C. E.; Davidovits, P.; Jayne, J. T.; Shi, Q.; Worsnop, D. R. *Prog. React. Kinet. Mech.* **2002**, *27*, 1−46.

(52) Worsnop, D. R.; Morris, J. W.; Shi, Q.; Davidovits, P.; Kolb, C. E. *Geophys. Res. Lett.* **2002**, *29*, 1996.

(53) Moise, T.; Rudich, Y. *J. Geophys. Res.* **2000**, *105*, 14667−14676.

(54) Martin, S. T. *Chem. Rev.* **2000**, *100*, 3403−3453.

(55) Markov, I. V. *Crystal Growth for Beginners*; World Scientific: Singapore, 1995.

(56) *Handbook of Crystal Growth*; Hurle, D. T. J., Ed.; Elsevier: Amsterdam, 1993; Vol. 1a.

(57) Inoue, T.; Hisatsugu, Y.; Ishikawa, R.; Suzuki, M. *Chem. Phys. Lipids* **2004**, *127*, 161−173.

(58) Kassner, K. *Pattern Formation in Diffusion-Limited Crystal Growth*; World Scientific: Singapore, 1996.

(59) Marcolli, C.; Luo, B. P.; Peter, T. *J. Phys. Chem. A* **2004**, *108*, 2216−2224.

(60) Cooke, W. F.; Ramaswamy, V.; Kasibhatla, P. *J. Geophys. Res.* **2002**, *107*, 4279.

(61) Chung, S. H.; Seinfeld, J. H. *J. Geophys. Res.* **2002**, *107*, 4407.

(62) Kinne, S.; Lohmann, U.; Feichter, J.; Schulz, M.; Timmreck, C.; Ghan, S.; Easter, R.; Chin, M.; Ginoux, P.; Takemura, T.; Tegen, I.; Koch,

D.; Herzog, M.; Penner, J.; Pitari, G.; Holben, B.; Eck, T.; Smirnov, A.; Dubovik, O.; Slutsker, I.; Tanre, D.; Torres, O.; Mishchenko, M.; Geogdzhayev, I.; Chu, D. A.; Kaufman, Y. *J. Geophys. Res.* **2003**, *108*, 4634.

(63) Lack, D. A.; Tie, X. X.; Bofinger, N. D.; Wiegand, A. N.; Madronich, S. *J. Geophys. Res.* **2004**, *109*, D03203.

(64) Schaap, M.; Van Der Gon, H.; Dentener, F. J.; Visschedijk, A. J. H.; Van Loon, M.; ten Brink, H. M.; Putaud, J. P.; Guillaume, B.; Liousse, C.; Builtjes, P. J. H. *J. Geophys. Res.* **2004**, *109*, D18207.

(65) Cooke, W. F.; Wilson, J. J. N. *J. Geophys. Res.* **1996**, *101*, 19395−19409.

(66) Saxena, P.; Hildemann, L. M.; McMurry, P. H.; Seinfeld, J. H. *J. Geophys. Res.* **1995**, *100*, 18755−18770.

(67) Saxena, P.; Hildemann, L. M. *J. Atmos. Chem.* **1996**, *24*, 57−109.

(68) Weingartner, E.; Burtscher, H.; Baltensperger, U. *Atmos. Environ.* **1997**, *31*, 2311−2327.

(69) Facchini, M. C.; Mircea, M.; Fuzzi, S.; Charlson, R. J. *Nature* **1999**, *401*, 257−259.

(70) Riemer, N.; Vogel, H.; Vogel, B. *Atmos. Chem. Phys.* **2004**, *4*, 1885−1893.

(71) Novakov, T.; Penner, J. E. *Nature* **1993**, *365*, 823−826.

(72) Novakov, T.; Corrigan, C. E. *Geophys. Res. Lett.* **1996**, *23*, 2141−2144.

(73) Lelieveld, J.; Crutzen, P. J.; Ramanathan, V.; Andreae, M. O.; Brenninkmeijer, C. A. M.; Campos, T.; Cass, G. R.; Dickerson, R. R.; Fischer, H.; de Gouw, J. A.; Hansel, A.; Jefferson, A.; Kley, D.; de Laat, A. T. J.; Lal, S.; Lawrence, M. G.; Lobert, J. M.; Mayol-Bracero, O. L.; Mitra, A. P.; Novakov, T.; Oltmans, S. J.; Prather, K. A.; Reiner, T.; Rodhe, H.; Scheeren, H. A.; Sikka, D.; Williams, J. *Science* **2001**, *291*, 1031−1036.

(74) Kaufman, Y. J.; Tanre, D.; Boucher, O. *Nature* **2002**, *419*, 215−223.